Sensors and Materials, Vol. 38, No. 2 (2026) 685–690
MYU Tokyo

S & M 4338

Synthesis of Low-temperature-phase X_1-Y_2SiO_5 Film Doped with Ce^{3+} and Its Luminescence Properties

Airi Shikichi and Akihiko Ito*

Graduate School of Environment and Information Sciences, Yokohama National University,
79-7 Tokiwadai, Hodogaya-ku, Yokohama 240-8501, Japan

(Received October 31, 2025; accepted December 22, 2025)

Keywords: X_1-Y_2SiO_5, chemical vapor deposition, thick film phosphor, scintillation properties

We synthesized low-temperature-phase X_1-Y_2SiO_5 doped with Ce^{3+} (Ce^{3+}:X_1-YSO) on a quartz glass substrate by laser-assisted chemical vapor deposition at a rate of 72 μm h^{-1}. Single-phase Ce^{3+}:X_1-YSO films were obtained at an Y_2O_3 molar ratio of 36 mol% in precursor vapor at a deposition temperature of 978–1079 K. Under UV irradiation, the Ce^{3+}:X_1-YSO film emitted a blue light originating from the 5d–4f transition of Ce^{3+} ions. Under 5.5 MeV α-ray excitation from an ^{241}Am source, the scintillation decay constant of the Ce^{3+}:X_1-YSO film was 22.9 ± 0.63 ns.

1. Introduction

Ce^{3+}-doped yttrium oxyorthosilicate (Ce^{3+}:Y_2SiO_5, Ce^{3+}:YSO) is a blue-emitting phosphor with a high relative density (4.45–4.74 g cm^{-3}), a high scintillation light yield (12410–26300 photons per MeV),[1,2] and a fast decay time [42–60 ns for single crystal bulk[3,4] and 22 ns for liquid phase epitaxy (LPE) film[5]]. These features make Ce^{3+}:YSO promising scintillator screens when made into films. Synthesis in film form has been achieved using methods such as LPE and pulsed laser deposition, but low deposition rates remain a challenge.[5–7] In the synthesis of films by the LPE method, impurities such as Pb^{2+} and Pt^{2+} from flux degraded the scintillation light yield of Ce^{3+}:YSO.[8] The chemical vapor deposition (CVD) method has been used to prepare YSO films; however, all studies have focused on environmental barrier coating applications, with no research yet conducted on scintillator applications.[9–11]

YSO has two different monoclinic crystal structures: the low-temperature X_1 phase (ICSD No. 51591; space group: $P2_1/c$ and a = 0.90139 nm, b = 0.69282 nm, c = 0.66427 nm) and the high-temperature X_2 phase (ICSD No. 27003; space group: $B2/b$ and a = 1.459 nm, b = 1.052 nm, c = 0.682 nm), with a phase transition occurring at 1463 K.[12] The crystal grown as a scintillator is the high-temperature X_2 phase, and reports on the scintillation properties of the low-temperature X_1 phase are limited to nanopowders synthesized by the sol-gel method.[13]

We focused on film deposition via laser-assisted chemical vapor deposition (LCVD). CVD enables crystal growth below the melting point or transition temperature, allowing the synthesis

*Corresponding author: e-mail: ito-akihiko-xr@ynu.ac.jp
https://doi.org/10.18494/SAM6098

ISSN 0914-4935
https://myukk.org/

of the low-temperature phase. Additionally, this method can be used for the high-speed synthesis of thick film phosphors,[14–16] and such a rapid production method can improve the production efficiency of Ce^{3+}:YSO thick film phosphors on quartz glass for scintillator screens. Synthetic quartz glass has high transmittance from the UV to NIR range and exhibits no clear scintillation luminescence, and it is cost-effective and readily available. In the present study, we prepared Ce^{3+}:X_1-YSO films on a quartz glass substrate by LCVD and investigated their microstructure and luminescence properties.

2. Materials and Methods

The LCVD apparatus has been described elsewhere.[17,18] Metal–organic compounds of tetraethyl orthosilicate (Shin-Etsu Chemical, Japan), yttrium tris(dipivaloylmethanate) (Strem Chemicals, USA), and cerium tetrakis(dipivaloylmethanate) [purity: 99.9%–Ce (REO)] (Strem Chemicals, USA) were maintained at temperatures of 318, 453–473, and 493 K, respectively, in precursor furnaces. The resultant vapor was transferred to a CVD chamber using Ar as the carrier gas, and O_2 gas was separately introduced to the chamber through a double-tubed nozzle. The molar ratio in the precursor vapor was estimated from the mass change in each precursor before and after deposition. The total chamber pressure was maintained at 150 Pa.

Quartz glass substrates ($5 \times 5 \times 0.5$ mm^3) polished on both sides were used. These substrates were preheated on a heating stage, then irradiated with a CO_2 laser (wavelength: 10.6 μm; maximum laser output: 60 W; SPT Laser Technology, China) through a ZnSe window. The laser irradiation heated the substrates to 868–1273 K. The deposition time was 0.6 ks.

The phase composition of the resultant film was determined by X-ray diffraction (XRD; Bruker D2 Phaser, USA). The microstructure was observed by scanning electron microscopy (SEM; JEOL JCM-6000, Japan). The photoluminescence (PL) and PL excitation (PLE) spectra were measured using a fluorescence spectrophotometer (JASCO FP-8300, Japan).

Details of the scintillation measurement are described elsewhere.[19] The ^{241}Am source was used as a 5.5 MeV α-ray and 60 keV γ-ray emitter.

3. Results and Discussion

Figure 1 shows the XRD patterns of the obtained films at various deposition temperatures (T_{dep}) and Y_2O_3 compositions in films ($C_{Y_2O_3}$). Single-phase X_1-YSO films were prepared on a quartz glass substrate at T_{dep} = 1078 K and $C_{Y_2O_3}$ = 35.5 mol% [Fig. 1(a)]. The films prepared from Si-rich composition, for example, at T_{dep} = 1073 K and $C_{Y_2O_3}$ = 24.6 mol%, formed a mixture of X_1 and X_2 phases [Fig. 1(b)], whereas some films prepared at a higher at T_{dep}, for example, at T_{dep} = 1171 K and $C_{Y_2O_3}$ = 39.0 mol%, showed the formation of a δ-yttrium pyrosilicate (δ-YPS) phase (ICSD No. 74778; space group: $Pna2_1$ and a = 1.36650 nm, b = 0.50166 nm, c = 0.81494 nm) [Fig. 1(c)].

Figure 2 shows the phase map constructed as a function of T_{dep} and $C_{Y_2O_3}$ for the obtained film. At T_{dep} = 800–1100 K, after increasing the Y_2O_3 molar ratio from 11.6 to 97.6 mol% in the precursor gas, the phase composition of the film changed from a four-phase mixture (X_1- and

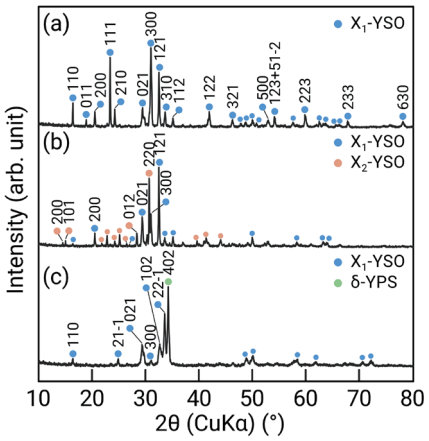

Fig. 1. (Color online) XRD patterns of films prepared on quartz glass substrates at (a) T_{dep} = 1078 K and $C_{Y_2O_3}$ = 35.5 mol%, (b) T_{dep} = 1073 K and $C_{Y_2O_3}$ = 24.6 mol%, and (c) T_{dep} = 1171 K and $C_{Y_2O_3}$ = 39.0 mol%.

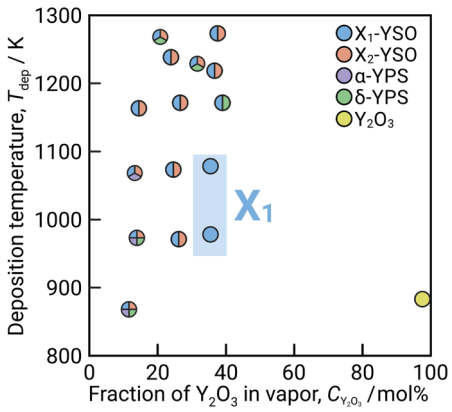

Fig. 2. (Color online) Phase map constructed as a function of T_{dep} and $C_{Y_2O_3}$ for the SiO_2–Y_2O_3 system films prepared on quartz glass substrate.

X_2-YSO and α- and δ-YPS) to a two-phase mixture (X_1- and X_2-YSO) to a single phase of X_1-YSO to cubic Y_2O_3. The single-phase Ce^{3+}:X_1-YSO films were obtained at $C_{Y_2O_3}$ = 36 mol% and T_{dep} = 978–1079 K. At T_{dep} = 800–1100 K, the films were a two- or three-phase mixture among X_1- and X_2-YSO and δ-YPS phases at $C_{Y_2O_3}$ = 20.7–39.0 mol%.

Figure 3 shows the cross-sectional and surface SEM images of the Ce^{3+}:X_1-YSO film prepared on a quartz glass substrate at T_{dep} = 1078 K and $C_{Y_2O_3}$ = 35.5 mol%. The cross section of the Ce^{3+}:X_1-YSO film exhibited a dense structure with a faceted surface [Figs. 3(a) and 3(b)]. The film was 12 μm thick, implying a deposition rate of 72 μm h^{-1}. The Ce^{3+} molar ratio in the film was measured to be 0.5 mol%. The film appeared colorless and translucent [Fig. 3(c)], and it emitted blue emissions under UV light irradiation [Fig. 3(d)].

Figure 4 shows the PL and PLE spectra of the Ce^{3+}:X_1-YSO film grown on a quartz glass substrate at T_{dep} = 1078 K and $C_{Y_2O_3}$ = 35.5 mol%. A raw quartz glass substrate showed no photoluminescence. The broad PL emission peak, centered at a wavelength of 420 nm, was attributed to the $5d \rightarrow {}^2F_{5/2}$ and $5d \rightarrow {}^2F_{7/2}$ transitions of Ce^{3+} ions in the X_1-YSO phase (solid line in Fig. 4). The PLE bands around 280 and 363 nm were contributed by energy transitions from the 4f state to the $5d_2$ and $5d_1$ states in Ce^{3+} ions, respectively (dashed line in Fig. 4).[20,21]

Figure 5 shows the scintillation decay curve under the 5.5 MeV α-ray excitation of the Ce^{3+}:X_1-YSO film. Assuming that the measured decay curve can be represented as the convolution of an instrument response factor approximated by a Gaussian function and the exponential fluorescence decay, the measured decay curves were fitted by an exponentially modified Gaussian function,[22,23]

$$\mathrm{EMG}(t) = h\sigma\sqrt{2\pi}(2\tau_1)\exp[(t_0 - t)/\tau_1 + \sigma^2/(2\tau_1{}^2)]\{|\tau_1|/\tau_1 - \mathrm{erf}[(t_0 - t)/\sqrt{2}\sigma + \sigma/\sqrt{2}\tau_1]\}, \quad (1)$$

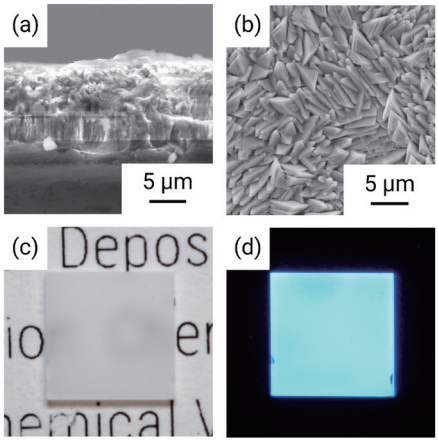

Fig. 3. (Color online) (a) Cross-sectional and (b) surface SEM images of the Ce^{3+}:X_1-YSO thick film grown on quartz glass substrate at T_{dep} = 1078 K and $C_{Y_2O_3}$ = 35.5 mol%. Photographs of the film under (c) room light and (d) UV light irradiation.

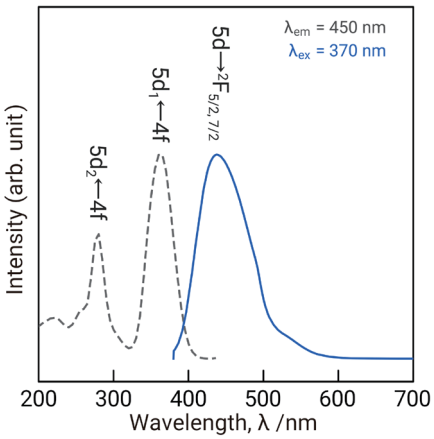

Fig. 4. (Color online) PLE spectrum of Ce^{3+}:X_1-YSO film monitored at λ_{em} = 450 nm (dashed line) and PL spectrum of the film excited at λ_{ex} = 370 nm (solid line).

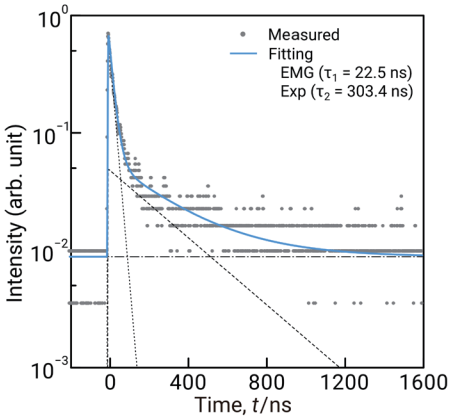

Fig. 5. (Color online) Scintillation decay curve of Ce^{3+}:X_1-YSO film under 5.5 MeV α-ray irradiation from the ^{241}Am source. The solid line indicates the total fitting model, which is the sum of the exponentially modified Gaussian function (dotted), exponential component (dashed), and constant for the baseline (dash-dotted).

where h, t_0, and σ are the Gaussian height, center, and width, respectively, and τ_1 represents a decay constant. The total fitting model is the sum of a constant for the baseline, the EMG(t) function, and an additional exponential component,

$$\mathrm{Exp}(t) = 1/\{1 + \exp[(t_0 - t)/a]\}\ A\ \exp(-t/\tau_2), \tag{2}$$

where A, a, and t_0 are the constant, gain, and time offset, respectively, and τ_2 represents a decay constant. To suppress divergence on the negative side of the exponential function and assume the rise of the exponential component, a sigmoid function, which is a function that closely approximates the result of convolving a step function with a Gaussian function, is multiplied by

the exponential function. The decay curve of the Ce^{3+}:X_1-YSO film was fitted using the Fityk software[24] with $h = 4.26$, $t_0 = -4.17$, $\sigma = 1.52$, $\tau_1 = 22.5$, $A = 0.05$, $a = 0.5$, and $\tau_2 = 303.4$, shown as solid lines in Fig. 5. The averaged fast and slow decay time constants were 22.9 ± 0.6 and 318.1 ± 33.7 ns, respectively.

In the YSO host lattice, Ce ions occupy two different Y sites. Ce_1 is usually designated to the Y site neighboring nine oxygens, and Ce_2 is designated to the Y site neighboring seven oxygens. Both Ce_1 and Ce_2 exhibit fast responses on the order of tens of nanoseconds (40–60 ns), whereas it has been reported that the coordination environment of Ce_2 shows a delayed decay on the order of 230 ns due to the thermally induced ionization of the excited state.[25] The slow decay time constant can be explained with this delayed decay process.

The measured fast decay constant was smaller than the reported values of 54–105 ns for the Ce^{3+}:X_1-YSO nanopowders prepared by the sol-gel method.[13] They reported that the decay time constant decreased from 105 to 54 ns as the sol-gel temperature increased from 1173 to 1523 K, suggesting that the crystallinity of the nanopowders might be insufficient. The present decay time constant of 22.9 ns was close to the reported value for the Ce^{3+}:X_2-YSO film (22 ns),[5] suggesting that the decay time constant of Ce^{3+}:X_1-YSO should be as short as that of Ce^{3+}:X_2-YSO.

In α-ray irradiation, the entire energy is imparted at a penetration depth of several to tens of micrometers due to the Coulomb interaction with matter. According to the SRIM simulation,[26] the Bragg length of a 5.5 MeV α-ray in YSO is 17.3 μm. At the center of the α-ray track, the density of electron–hole pairs and excitons becomes extremely high. This causes the shallow traps surrounding the track to be instantly filled with electrons. Overflowing carriers then proceed directly toward the luminescence center without being affected by the traps. This results in the dominant component being the fast component, or the carriers may be quenched owing to interactions between highly dense excited states. This process may have contributed to the fast response of the Ce^{3+} center. Rothfuss *et al*. investigated the decay behavior of the Ce^{3+}:YSO single crystal bulk under α- and γ-ray irradiations.[4] Although the α-ray irradiation resulted in a sharp peak rise due to the high linear energy transfer, the decay became slower than γ-ray irradiation. On the other hand, in the α-ray irradiation in narrow regions such as film scintillators, the high linear energy transfer may contribute to an accelerated decay response.

4. Conclusions

We synthesized Ce^{3+}:X_1-YSO films on a quartz glass substrate by laser-assisted CVD. The single-phase Ce^{3+}:X_1-YSO films were obtained at $C_{Y_2O_3}$ = 36 mol% and T_{dep} = 978–1079 K. Under the Si-rich condition, the films were three- or four-phase mixtures among X_1- and X_2-YSO and α- and δ-YPS phases, whereas at high deposition temperatures, the films were two- or three-phase mixtures among X_1- and X_2-YSO and δ-YPS phases. Under UV irradiation, the Ce^{3+}:X_1-YSO films emitted blue light at 400–500 nm, originating from the 5d–4f transitions of the Ce^{3+} centers. The fast decay time constant of the Ce^{3+}:X_1-YSO film for the 5.5 MeV α-ray irradiation was 22.9 ± 0.6 ns, which was smaller than the reported values of Ce^{3+}:X_1-YSO powders but was comparable to the reported values of Ce^{3+}:X_2-YSO.

Acknowledgments

This work was supported in part by JSPS KAKENHI Grant Numbers 21H05199, 24K91211, 24K21685, 24K21746, and 25H00796.

References

1 K. Wantong, N. Yawai, W. Chewpraditkul, M. Kucera, M. Hanus, and M. Nikl: J. Cryst. Growth **468** (2017) 275. https://doi.org/10.1016/j.jcrysgro.2016.12.094
2 C. Wanarak, A. Phunpueok, and W. Chewpraditkul: Nucl. Instrum. Methods Phys. Res. Sect. B **286** (2012) 72. https://doi.org/10.1016/j.nimb.2011.11.028
3 C. L. Melcher, R. A. Manente, C. A. Peterson, and J. S. Schweitzer: J. Cryst. Growth **128** (1993) 1001. https://doi.org/10.1016/S0022-0248(07)80086-8
4 H. E. Rothfuss, C. L. Melcher, L. Eriksson, M. Eriksson, and R. Grazioso: 2007 IEEE Nuclear Science Symp. Conf. Record (IEEE, 2007) 1401–1403. https://doi.org/10.1109/NSSMIC.2007.4437261
5 Yu. Zorenko, V. Gorbenko, V. Savchyn, T. Zorenko, B. Grinyov, O. Sidletskiy, A. Fedorov, J. A. Mares, M. Nikl, and M. Kucera: Radiat. Meas. **56** (2013) 84. https://doi.org/10.1016/j.radmeas.2013.05.004
6 E. Coetsee, J. J. Terblans, and H. C. Swart: Phys. B Condens. Matter **404** (2009) 4431. https://doi.org/10.1016/j.physb.2009.09.046
7 E. Coetsee, H. C. Swart, J. J. Terblans, O. M. Ntwaeaborwa, K. T. Hillie, W. A. Jordaan, and U. Buttner: Opt. Mater. **29** (2007) 1338. https://doi.org/10.1016/j.optmat.2006.06.009
8 Yu. Zorenko, V. Gorbenko, V. Savchyn, T. Voznyak, V. V. Gorbenko, M. Nikl, J. A. Mares, O. Sidletskiy, B. Grynyov, A. Fedorov, K. Fabisiak, and K. Paprocki: Opt. Mater. **34** (2012) 1969. https://doi.org/10.1016/j.optmat.2011.11.021
9 A. Ito, J. Endo, T. Kimura, and T. Goto: Mater. Chem. Phys. **125** (2011) 242. https://doi.org/10.1016/j.matchemphys.2010.09.014
10 A. Ito, J. Endo, T. Kimura, and T. Goto: Surf. Coat. Technol. **204** (2010) 3846. https://doi.org/10.1016/j.surfcoat.2010.04.066
11 F. He, Y. Liu, Y. Gao, J. Wang, and C. Zhang: Ceram. Int. **46** (2020) 27973. https://doi.org/10.1016/j.ceramint.2020.07.291
12 E. J. Bosze, J. McKittrick, and G. A. Hirata: Mater. Sci. Eng. B **97** (2003) 265. https://doi.org/10.1016/S0921-5107(02)00598-6
13 B. Zahra, L. Guerbous, M. S. E. Hamroun, and H. Mekki: Appl. Radiat. Isot. **225** (2025) 111956. https://doi.org/10.1016/j.apradiso.2025.111956
14 S. Matsumoto and A. Ito: Sci. Rep. **12** (2022) 19319. https://doi.org/10.1038/s41598-022-23839-w
15 S. Matsumoto, A. Minamino, and A. Ito: Sens. Mater. **33** (2021) 2209. https://doi.org/10.18494/SAM.2021.3325
16 S. Matsumoto, T. Watanabe, and A. Ito: Sens. Mater. **34** (2022) 669. https://doi.org/10.18494/SAM3698
17 A. Ito, H. Kadokura, T. Kimura, and T. Goto: J. Alloys Compd. **489** (2010) 469. https://doi.org/10.1016/j.jallcom.2009.09.088
18 A. Ito: J. Ceram. Soc. Jpn. **129** (2021) 646. https://doi.org/10.2109/jcersj2.21135
19 Y. Deguchi and A. Ito: Opt. Mater. **153** (2024) 115565. https://doi.org/10.1016/j.optmat.2024.115565
20 L. Wang, Z. Hou, Z. Quan, C. Li, J. Yang, H. Lian, P. Yang, and J. Lin: Inorg. Chem. **48** (2009) 6731. https://doi.org/10.1021/ic9006789
21 T. Aitasalo, J. Hölsä, M. Lastusaari, J. Niittykoski, and F. Pellé: Opt. Mater. **27** (2005) 1511. https://doi.org/10.1016/j.optmat.2005.01.009
22 T. Nakayama, S. Kurosawa, and A. Ito: J. Lumin. **288** (2025) 121589. https://doi.org/10.1016/j.jlumin.2025.121589
23 T. Oga, S. Kurosawa, and A. Ito: J. Lumin. **288** (2025) 121568. https://doi.org/10.1016/j.jlumin.2025.121568
24 M. Wojdyr: J. Appl. Crystallogr. **43** (2010) 1126. https://doi.org/10.1107/S0021889810030499
25 V. Jary, M. Nikl, G. Ren, P. Horodysky, G. P. Pazzi, and R. Kucerkova: Opt. Mater. **34** (2011) 428. https://doi.org/10.1016/j.optmat.2011.04.034
26 J. F. Ziegler, M. D. Ziegler, and J. P. Biersack: Nucl. Instrum. Methods Phys. Res. Sect. B **268** (2010) 1818. https://doi.org/10.1016/j.nimb.2010.02.091